

1 **Dynamic analysis of drought propagation in the context of**
2 **climate change and watershed characterization: a quantitative**
3 **study based on GAMLSS and Copula models**

4 Min Li^{1,2,*}, Zilong Feng¹, Mingfeng Zhang³, Lijie Shi¹, Yuhang Yao¹

5 ¹College of Hydraulic Science and Engineering, Yangzhou University, Yangzhou 225000,
6 China

7 ²Key Laboratory of Flood & Drought Disaster Defense, the Ministry of Water Resources,
8 Nanjing 210029, China

9 ³Guangxi Hydraulic Research Institute, Nanning, China

10 *Correspondence to:* Min Li, (limintju@126.com)

11 **Abstract:** The analysis of the law of drought propagation under a changing environment is of great significance
12 for drought early warning and reducing social and economic losses. Currently, few studies have analyzed the
13 effects of meteorological factor and watershed characteristics on drought propagation based on non-stationary
14 drought indices. In this paper, the probabilities and thresholds of meteorological drought to hydrological drought
15 propagation were calculated using the non-stationary drought index constructed using the Generalized Additive
16 Model for Location, Scale, and Shape (GAMLSS) model and the Copula function to assess the influence of
17 large-scale climatic indices, meteorological elements, and watershed characteristics on the propagation
18 characteristics of seasonal droughts. The results showed that non-stationary drought indices that incorporate
19 meteorological factors tended to have better performance than standardized drought indices. Under the combined
20 influence of large-scale climatic indices, temperature, specific humidity, and wind speed, the propagation
21 probabilities became larger especially during spring and winter in the upstream and midstream regions, with the
22 propagation thresholds in winter significantly increasing by 0.1-0.2. These mean that hydrologic droughts are
23 more likely to be triggered. Furthermore, watershed characteristics also be factors influencing spatial differences
24 in drought propagation.

25 **Keywords:** Climate change; Watershed characteristics; Drought propagation; Luanhe River basin

26 **1. Introduction**

27 As one of the major climate problems, meteorological drought poses a serious threat to the ecological

28 environment and social economy (Wang et al. 2022; Hao et al. 2019; Kumar et al. 2019). In a drought event,
29 meteorological drought often occurs first and insufficient precipitation leads to hydrological drought or
30 agricultural drought through the hydrological cycle (Han et al. 2019; Zhang et al. 2022; Zhong et al. 2020). This
31 evolution from one drought to another is called drought propagation (Zhang et al. 2021; Wossenyeleh et al. 2021;
32 Apurv and Cai 2020; Jehanzaib et al. 2020). After suffering from numerous drought disasters, it is widely
33 recognized that the impact of drought on human life can be reduced by investigating the propagation of droughts.
34 (Pandey et al. 2022; Dehghani et al. 2019; Le et al. 2016).

35 Drought is often studied based on drought indices, and the choice of drought index is crucial for
36 characterizing regional drought (Mahmoudi et al. 2019; Tao et al. 2021; Xu et al. 2021). Some drought indices:
37 the Standardized Precipitation Index (SPI), the Standardized Precipitation Evapotranspiration Index (SPEI), the
38 Standardized Runoff Index (SRI) and the Standardized Soil moisture Index (SSI) are used to describe the
39 drought characteristics of a region (McKee et al. 1993; Vicente-Serrano et al. 2010; Shukla and Wood 2008; Xu
40 et al. 2021). In recent years, scholars have made a lot of efforts to examine drought propagation characteristics,
41 employing a wide range of analytical tools including both statistical analyses and model simulations. such as the
42 Copula models (Wu et al. 2022; Wang et al. 2022; Guo et al. 2020), Markov (Yeh and Hsu 2019; Vorobevskii et
43 al. 2022), and Variable Infiltration Capacity (VIC) model (Bhardwaj et al. 2020; Lilhare et al. 2020). Wang et al.
44 (2022) analyzed the propagation probability characteristics of meteorological drought to hydrological drought in
45 the Yiluo River Basin based on the copula function. Sattar et al. (2020) assessed the propagation probability of
46 meteorological drought to different categories of hydrological drought in the Han River basin using Markov
47 Bayesian Classifier and conditional probabilities. Bhardwaj et al. (2020) assessed drought propagation
48 characteristics in India based on the SPI and VIC models.

49 Some studies have shown that under the dual influence of climate change and human activities, the
50 spatiotemporal evolution characteristics of drought are difficult to analyze (Wu et al. 2022; Jehanzaib et al. 2020;
51 Zhou et al. 2019). Therefore, scholars analyzed the factors that affect the propagation of droughts around the
52 world (Li et al. 2019b). For instance, Jehanzaib et al. (2020) and Peña-Gallardo et al. (2019) have found that
53 climate type, climate change, catchment characteristics, and other factors can affect the propagation of drought.
54 Ding et al. (2021) showed the effect of climate on drought propagation by comparing the differences in
55 propagation time from meteorological drought to hydrological drought in different climatic regions of China.
56 Guo et al. (2021) assessed the impact of large reservoirs on propagation by comparing differences in drought
57 propagation characteristics before and after reservoir construction.

58 Under the influence of factors such as climate change and human activities, precipitation and runoff series
59 show significant non-stationarity and uncertainty, and drought studies have become more complex and urgent
60 (Wang et al. 2015; Wang et al. 2020; Jehanzaib et al. 2023). Therefore, researchers incorporate non-stationarity
61 into drought studies through more appropriate analytical tools, The GAMLSS model is one of the commonly
62 used methods. Previously, researchers mostly used the non-stationary drought index constructed based on the
63 GAMLSS model to assess the impacts of climate change, human activities, and other factors on a single drought,
64 indicating that the non-stationary drought indices have a better performance than the stationary drought index in
65 drought research (Shao et al. 2022; Wang et al. 2023). Since then, the non-stationary drought indices have been
66 gradually applied to the study of drought propagation. Das et al. (2022) constructed non-stationary
67 meteorological and hydrological drought indices using large-scale climatic factors and regional meteorological
68 elements as covariates for precipitation and runoff, respectively, and assessed the impact of external drivers on
69 drought propagation characteristics. Overall, fewer studies incorporate non-stationary drought indices into
70 drought propagation.

71 As the main source of water supply for the Beijing-Tianjin-Tangshan area, the Luanhe River Basin is
72 responsible for multiple tasks such as urban water supply, and industrial and agricultural water supply. Frequent
73 droughts in recent years have not only affected the supply of regional water resources but also had a serious
74 impact on the ecological environment. Therefore, an in-depth understanding of the evolution pattern and impact
75 mechanism of drought is of great significance to the rational allocation of water resources and sustainable
76 development of the basin. According to some recent studies, there are nonstationary characteristics in the
77 precipitation series and the runoff series of the Luanhe River Basin (Li et al. 2019a; Li et al. 2020). And the
78 occurrence of the drought in Luanhe River Basin may be related to some large-scale climatic indices (Wang et al.
79 2018; Li et al. 2015; Wang et al. 2016). Previous studies on the Luanhe River Basin have focused on examining
80 the effects of large-scale climatic factors on a single type of drought, with few assessments of the effects of
81 large-scale climatic indices and regional meteorological elements on drought propagation (Li et al. 2015; Wang
82 et al. 2015; Li et al. 2024).

83 Although some progress has been made in the study of drought propagation, there are few studies
84 considering the impact of changing environments. Furthermore, spatial and temporal differences in drought
85 propagation also be strongly related to watershed characteristics. To assess the impact of external drivers on
86 drought propagation, the GAMLSS framework with climate factors as covariates and copula model were
87 constructed to calculate the propagation probabilities and propagation thresholds from meteorological drought to

88 hydrological drought under stationary and non-stationary conditions in different seasons in this paper,
89 respectively. The effects of climate change on drought propagation were quantified at a seasonal scale, and the
90 impacts of watershed characteristics on drought propagation were explored.

91 **2. Study area and data**

92 The Luanhe River is the second largest river in Hebei Province, China, and its geographical location is
93 shown in Fig. 1(a). The area of the basin is about 44800 km², with an average width of 90km from east to west
94 and a length of 500km from north to south, including mountain 44070 km² and plain 810 km². There are obvious
95 differences in physical and geographical conditions, and the topography of the whole basin is high in the
96 northwest and low in the southeast.

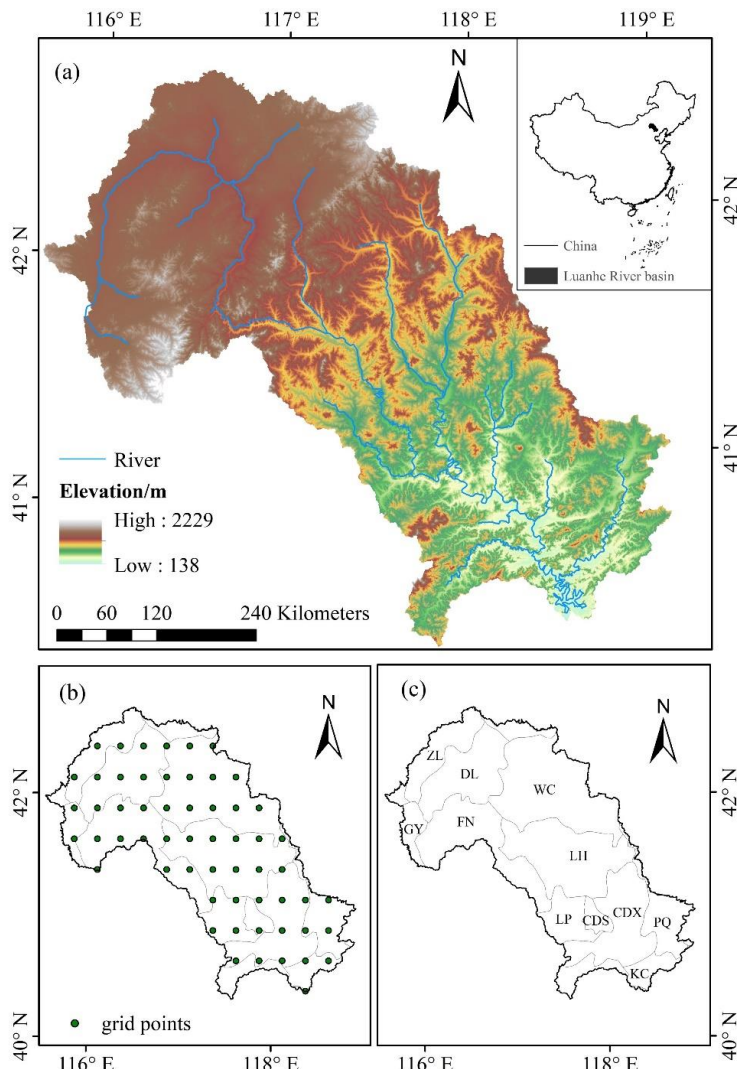
97 The surface is flat and the river valley is wide and shallow in the Luanhe River basin. The climate
98 difference between the north and south of the Luanhe River basin is obvious. The annual mean temperature
99 ranges from 1 to 11°C, and the monthly mean temperature ranges from 17 to 25°C. Affected by the continental
100 monsoon climate, the basin has four distinct seasons of precipitation, with an average annual precipitation of
101 400~800mm, of which summer precipitation accounts for 67%-76% of the total annual precipitation; spring and
102 autumn account for about 9% and 15% respectively; and winter precipitation accounts for only about 2% (Li et
103 al. 2023). The climate type changes from cold temperate arid and semi-arid climate to warm temperate semi-
104 humid climate.

105 With global climate change, drought disasters in the Luanhe River Basin are becoming increasingly
106 frequent, causing serious losses to the region's ecology and socio-economy. According to historical records
107 (Chen et al. 2019; Chen et al. 2022; Li and Zhou 2016), the main drought events in the Luanhe River Basin
108 occurred in 1961, 1963, 1968, 1972, 1980-1984, 2000, 2007, and 2009. The cumulative economic losses caused
109 by drought disasters in the basin during the period from 1960 to 2010 exceeded 13 billion yuan. Under the
110 influence of climate change and human activities, the evolution law and propagation characteristics of drought in
111 the basin become more complex.

112 In this paper, the large-scale climatic indices (abbreviated as CI) Nino3.4, Atlantic Multidecadal Oscillation
113 (AMO), Southern Oscillation Index (SOI), Pacific Decadal Oscillation (PDO), Arctic Oscillation (AO), North
114 Atlantic Oscillation (NAO) and North Pacific (NP) data are derived from the National Oceanic and Atmospheric
115 Administration (NOAA) (<http://www.esrl.noaa.gov/psd/data/climateindices>) (1960-2014). The average monthly

116 precipitation, temperature, wind speed, specific humidity, evapotranspiration, and runoff datasets are available at
 117 a grid resolution of 0.25° Lat \times 0.25° Lon are obtained from
 118 https://disc.gsfc.nasa.gov/datasets/GLDAS_NOAH10_M_2.0/. The grid-wise analysis is carried out at a
 119 resolution of 0.25° Lat \times 0.25° Lon over The Luanhe River that includes 58 grid points (Fig. 1(b)). Leaf area
 120 index of 0.25° spatial resolution was derived from the Advanced Very High Resolution Radiometer (AVHRR)
 121 Global Inventory Modeling and Mapping Studies (GIMMS) LAI3g version 2 (<https://daac.ornl.gov/>) (1981–
 122 2015).

123

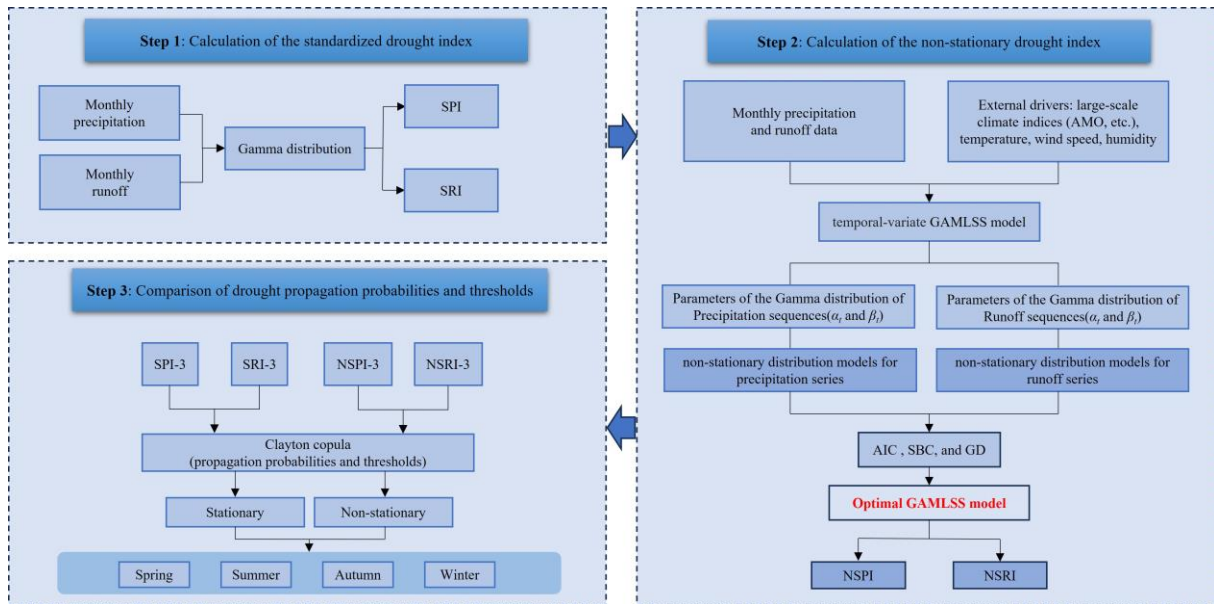


124 **Figure 1 The geographical location of the Luanhe River Basin (a), and the grid points contained in the**
 125 **watershed boundaries (b), 11 subregions contained in the watershed (c)**

126 **3. Methods**

127 The current study aims to assess the impact of external drivers on drought propagation based on the

128 GAMLSS model, in particular, the probability and threshold of drought propagation in different seasons. Figure
 129 3 summarizes the steps of the current study.



131 **Figure 2 Flowchart of this study**

132 **3.1 Pearson correlation test**

133 Pearson correlation test can be used to test whether there is a correlation between two sample sequences that
 134 follow a normal distribution. The formula is as follows:

$$135 \quad t = \frac{\gamma_{xy} \sqrt{n-2}}{\sqrt{1-\gamma_{xy}^2}} \quad (1)$$

136 Where n is the length of the test sample sequence, represent two different sequences, and the correlation
 137 coefficient is calculated as follows:

$$138 \quad \gamma_{xy} = \frac{\sum_{i=1}^n (x_i - \bar{x}) \cdot (y_i - \bar{y})}{\sqrt{\sum_{i=1}^n (x_i - \bar{x})^2 \cdot \sum_{i=1}^n (y_i - \bar{y})^2}} \quad (2)$$

139 Here, the range of γ_{xy} values is $[-1, 1]$, and when the value $|\gamma_{xy}|$ is close to 1 (Kang et al. 2022), the
 140 correlation between the two variables is higher.

141 Usually, there is more than one climate factor affecting meteorological drought (Gao et al. 2020). In this
 142 paper, Pearson correlation is used to test the correlation between large-scale climate indices and precipitation

143 series, to select the relevant climate variables. The wind speed, temperature, and specific humidity are
 144 considered the main influencing factors of watershed runoff.

145 **3.2 The calculation of drought index**

146 Generalized Additive Models for Location, Scale, and Shape (GAMLSS) proposed by Rigby and
 147 Stasinopoulos (2005) can flexibly analyze non-stationary time series, more details of GAMLSS are available in
 148 Rigby et al. (2005). The semi-parametric additive model formula used in this study is as follows:

149

$$g_1(\alpha_t) = \sum_{j=1}^{j_k} h_{jk}(c_{jk}) \quad (3)$$

150

$$g_2(\beta_t) = \sum_{j=1}^{j_k} h_{jk}(c_{jk}) \quad (4)$$

151 Where $g_1(\alpha_t)$ is the link function, which is determined by the domain of the statistical parameter, namely,
 152 if the domain of the distributed parameter α_t is $\alpha_t \in R$, the link function is $g_1(\alpha_t) = \alpha_t$, if $\alpha_t > 0$, then
 153 $g_1(\alpha_t) = \ln \alpha_t$. The h_{jk} represents the dependence function of the distribution parameters on the covariates
 154 c_{jk} . The parameter coefficients and model residuals are estimated by RS algorithm, and whether the model
 155 residuals approximately satisfy the normal distribution is analyzed, and the optimal fitting distribution is selected
 156 by the AIC (Akaike information criterion), SBC (Schwarz Bayesian Criterion), and GD (Global Deviance).

157 **3.2.1 Stationary Model**

158 Taking precipitation as the object and based on the principle of hydrological calculation and normal
 159 standardization method, SPI has the advantages of convenient data collection, relatively simple calculation,
 160 suitable for multi-spatiotemporal scale calculation. Suppose that the precipitation series X at a certain time scale
 161 satisfies the probability density function of Gamma distribution $f(x)$:

162

$$f(x) = \frac{x^{\alpha-1} e^{-x/\beta}}{\beta^\alpha \Gamma(\alpha)} \quad (5)$$

163 In the formula, α and β are scale and shape parameters ($\alpha > 0$, $\beta > 0$) and they are treated as constants in
 164 the GAMLSS framework. The cumulative probability of precipitation is as follows:

165

$$F(x) = \int_0^x f(x) dx \quad (6)$$

166 The corresponding SPI is obtained by normalizing the cumulative probability $F(x)$ of each item.

167 If $0 < F(X) \leq 0.5$:

168

$$k = \sqrt{\ln \left[\frac{1}{F^2(x)} \right]} \quad (7)$$

169
$$\text{SPI} = -k - \left(\frac{c_0 + c_1 k + c_2 k^2}{1 + d_1 k + d_2 k^2 + d_3 k^3} \right) \quad (8)$$

170 If $0.5 < F(X) \leq 1$:

171
$$k = \sqrt{\ln \frac{1}{[1 - F(x)]^2}} \quad (9)$$

172
$$\text{SPI} = k - \left(\frac{c_0 + c_1 k + c_2 k^2}{1 + d_1 k + d_2 k^2 + d_3 k^3} \right) \quad (10)$$

173 Here: $c_0 = 2.515517$, $c_1 = 0.802853$, $c_2 = 0.010328$, $d_1 = 1.4132788$, $d_2 = 0.189269$ and

174 $d_3 = 0.001308$.

175 As a drought index that can effectively and accurately describe the hydrological drought characteristics of
176 the basin, SRI can be calculated by replacing the precipitation sequence with the runoff sequence and the
177 calculation method of SRI is similar to that of SPI. Table 1 shows the drought class classification (Kolachian and
178 Saghafian 2021).

179 **Table 1 Drought class classification and corresponding SPI values and SRI value**

SPI\SRI value	Class
> -0.5	Normal
-0.5 to -1.00	Mild
-1.00 to -1.50	Moderate
-1.50 to -2.00	Severe
≤ -2.00	Extreme

180 **3.2.2 Nonstationary Model**

181 The non-stationary modeling is based on the study by Das et al. (2022). To better study the seasonal
182 characteristics of drought and capture the changes in meteorological elements caused by seasonal climate change,
183 this paper chooses the drought index on a 3-month time scale to analyze the propagation characteristics of
184 drought, and the GAMLSS model is used to construct a non-stationary model for the analysis of precipitation
185 and runoff changes. By incorporating large-scale climate factors as covariates, a non-stationary meteorological
186 drought index is constructed and used to capture the non-stationary characteristics of precipitation series in the
187 basin. In this paper, assuming that the precipitation series at a certain time scale satisfies the gamma function
188 distribution, the cumulative probability is as follows:

189
$$F_t(x) = \int_0^x \frac{x^{\alpha_t - 1} e^{-x/\beta_t}}{\beta_t^{\alpha_t} \Gamma(\alpha_t)} dx \quad (11)$$

190 α_t and β_t are the scale and position parameters of the gamma distribution. The correlated climate
 191 variables are selected from these large-scale climate factors (e.g., AMO, SOI, PDO, AO, NAO, and NP). The
 192 distribution of the probability density function can be fitted by the GAMLSS framework.

193 To capture the non-stationary characteristics of the basin runoff sequence, the non-stationary hydrological
 194 drought index (NSRI) was constructed. The meteorological variables (wind speed, temperature, and specific
 195 humidity) were considered as covariates for non-stationary modeling.

196 **3.3 The Copula model**

197 In multivariate drought probability analysis, the Copula function is an effective tool for constructing
 198 multivariate joint drought distributions with multiple characteristics based on the univariate distribution and the
 199 linkage structure between random variables. The equation is expressed as follows:

$$200 \quad C(u, v) = \varphi^{-1}(\varphi(u), \varphi(v)) \quad (12)$$

201 where $C(u, v)$ is the Copula function that combines two random variables, φ is the convex function, u
 202 and v represent the two variables respectively. Before establishing the joint distribution, the marginal
 203 distribution of the random variables needs to be determined, and in this study, the normal distribution is used as
 204 the marginal distribution of the meteorological drought index and hydrological drought index series. Droughts
 205 are usually extreme climatic events, precipitation shortages and other extreme conditions, which are statistically
 206 manifested in the behavior of data tails. And Clayton Copula can effectively capture the tail correlation between
 207 variables, which is especially significant in the research of drought. Therefore, Clayton Copula is used to
 208 construct the joint distribution between meteorological drought and hydrological drought indices in this paper
 209 (Guo et al. 2021; Zhang et al. 2022; Zhang et al. 2023). Based on the Copula model, the conditional probabilities
 210 are calculated as follows (Liu et al. 2022):

$$211 \quad P[W \leq v / Z \leq u] = \frac{P(Z \leq u, W \leq v)}{P(Z \leq u)} = 1 - \frac{w(v) - C(z(u), w(v))}{1 - z(u)} \quad (13)$$

212 Here $Z(z_1, z_2, \dots, z_n)$ is the conditional variable, $W(w_1, w_2, \dots, w_n)$ is the target variable, and $z(u)$ is
 213 used to denote the cumulative probability of $Z \geq u$, $w(v)$ denotes the cumulative probability of $W \geq v$, and
 214 $C(z(u), w(v))$ is the joint cumulative probability. In this paper, with the meteorological drought index as the
 215 condition and the hydrological drought index as the target, then $P[W \leq v / Z \leq u]$ denotes the conditional
 216 probability of occurrence of hydrological drought under different meteorological drought conditions.

217 The drought propagation threshold (PT) is commonly defined as the severity of the meteorological drought
 218 that is most likely to cause hydrological drought, i.e., the SPI critical threshold. In this paper, the conditional
 219 probability density of SPI was calculated for each scenario in the interval of -3 to 3 at an interval of 0.01, and
 220 when $SRI \leq -0.5$, the SPI value corresponding to the maximum point of the conditional probability density is the
 221 meteorological drought threshold that triggers hydrological drought (Zhou et al. 2022).

222 To visualize more intuitively the difference between meteorological drought to hydrological drought
 223 propagation thresholds under non-stationary and stationary condition, the change rate of drought propagation
 224 thresholds was calculated with the following equations:

225

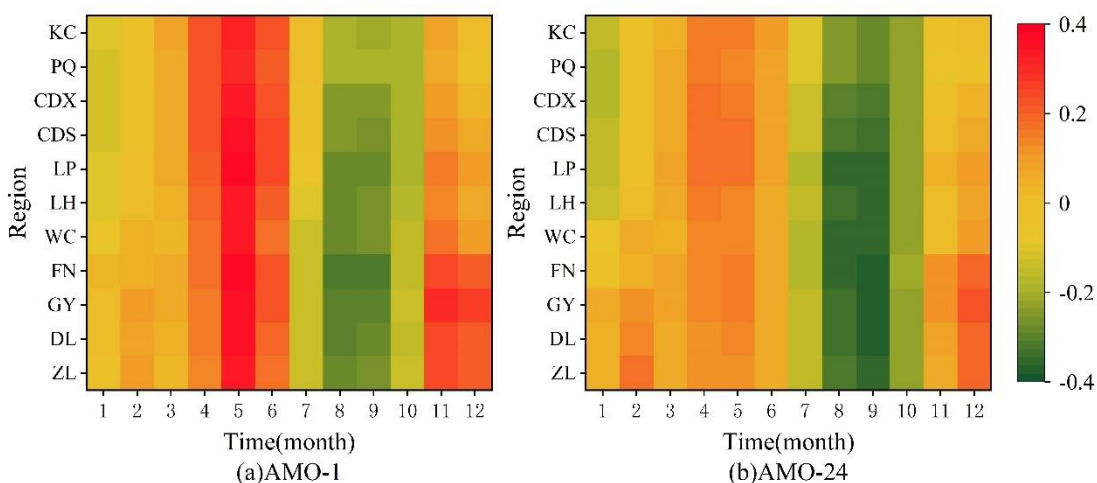
$$R_c = \left| \frac{T_n - T_s}{T_s} \right| \times 100\% \quad (14)$$

226 where T_n and T_s the thresholds of meteorological drought to hydrological drought propagation under non-
227 stationary conditions and stationary conditions.

228 **4. Results**

229 **4.1 Selection of Climate Indices**

230 To select the relevant climate variables linked with meteorological drought in the Luanhe River basin, the
231 Pearson correlation test was carried out to test the correlation between cumulative precipitation series at different
232 time scales K ($K = 1, 3, 6, 12, 24$ months) and the CI with a lead time M ($M = 0, 1, 2, 3$ months) for all regions
233 of the basin. The standardized climatic indices series have been averaged on a period (AP) of 1, 3, 6, 12, and 24
234 months ($CI-n$: CI with the $AP=n$ month). To analyze the seasonal drought characteristics of the basin, we
235 selected the significant climate indices for the cumulative precipitation series on a three-month time scale.
236 According to the results of the correlation test, AMO-1 and AMO-24 with a lead time of $M=0$ months were
237 selected as covariates for the precipitation series and the test results are shown in Fig. 3.



239 **Figure 3 The correlation between AMO and precipitation series**

240 Trends of temperature, wind speed, and humidity in different seasons were calculated by the Mann-Kendall
241 (M-K) trend analysis method in the watershed (Mann 1945; Cheng et al. 2023). The results are presented in
242 Table 2. When the absolute value of Z is greater than 1.96, it indicates that the series shows a significant level of
243 $p < 0.05$. The temperature shows a significant upward trend in four seasons. Wind speed shows a decreasing

244 trend in spring and summer and an increasing trend in autumn and winter. Relative humidity showed an
 245 increasing trend in spring, summer, and winter, and a decreasing trend in summer.

246 **Table 2 Trends of temperature, wind speed, and specific humidity in different seasons (The bold numbers**
 247 **represent the series shows a significant trend.)**

	Z			
	Spring	Summer	Autumn	Winter
Temperature	4.55	4.37	4.13	3.66
Wind speed	-0.03	-4.21	0.12	0.58
Specific humidity	1.29	-0.07	1.10	2.61

248 **4.2 Preference of GAMLSS model**

249 **4.2.1 The simulation of precipitation series**

250 GAMLSS framework was used to model the precipitation in each region of the watershed. To analyze the
 251 seasonal drought characteristics of the region, the SPI was calculated for 3-month time scales in this article.
 252 According to the correlation test results, AMO (AP=1 and AP=24) was selected as the significant *CI* for non-
 253 stationary modeling of precipitation. Seven different situations were considered according to the structure of the
 254 GAMLSS model (the model types are shown in Table 3). The AIC, SBC, and GD were used to select the optimal
 255 model, taking the CDS region as an example, the results of model preferences for the precipitation series are
 256 shown in Table 3.

257 **Table 3 Different model situations considered for precipitation simulation (CI-n: CI with the AP=n month)**

Model	Parameters	
	α_t	β_t
Mod 1	~1	~1
Mod 2	~1	~AMO-1, AMO-24
Mod 3	~ AMO-1, AMO-24	~1
Mod 4	~1	~ AMO-24
Mod 5	~ AMO-24	~1
Mod 6	~1	~ AMO-1
Mod 7	~ AMO-1	~1

258 **Table 4 AIC, SBC, and GD of the different models of precipitation in the CDS region (the Bold indicates**
 259 **the optimal model)**

Model	Spring			Summer			Autumn			Winter		
	AIC	SBC	GD	AIC	SBC	GD	AIC	SBC	GD	AIC	SBC	GD
Mod 1	498.2	502.2	494.2	626.8	630.7	622.8	505.8	509.7	501.8	325.3	329.3	321.3

Mod2	501.7	509.6	493.7	629.2	637.1	621.2	509.4	517.3	501.4	322.5	330.4	314.5
Mod3	495.1	503.0	487.1	627.7	635.6	619.7	508.3	516.2	500.3	329.3	337.1	321.3
Mod4	500.0	506.0	494.0	627.2	633.1	621.2	507.7	513.6	501.7	329.9	324.0	318.0
Mod5	499.1	505.0	493.1	625.8	631.7	619.8	507.8	507.8	513.7	327.3	333.2	321.3
Mod6	500.2	506.1	494.2	627.6	633.5	621.6	507.8	513.7	501.8	327.2	333.1	321.2
Mod7	494.1	500.0	488.1	627.6	633.5	621.6	507.2	513.1	501.2	327.3	333.2	321.3

260 As can be seen from Table 4, for the non-stationary models of precipitation in the CDS region, among all
 261 the models with climate index as covariates, Mod7 has the best performance in spring, with the AIC, SBC, and
 262 GD of 494.1, 500.0 and 488.1 respectively. The optimal model in summer was Mod5, the AIC, SBC, and GD
 263 were 625.8, 631.7, and 619.8. In autumn, the optimal model was Mod1, the AIC, SBC, and GD were 505.8,
 264 509.7, and 501.8. Mod2 had the best performance in winter, with the AIC, SBC, and GD of 322.5, 330.4, and
 265 314.5. The results of the estimated model parameters of the precipitation in the CDS region are shown in Table 5:
 266

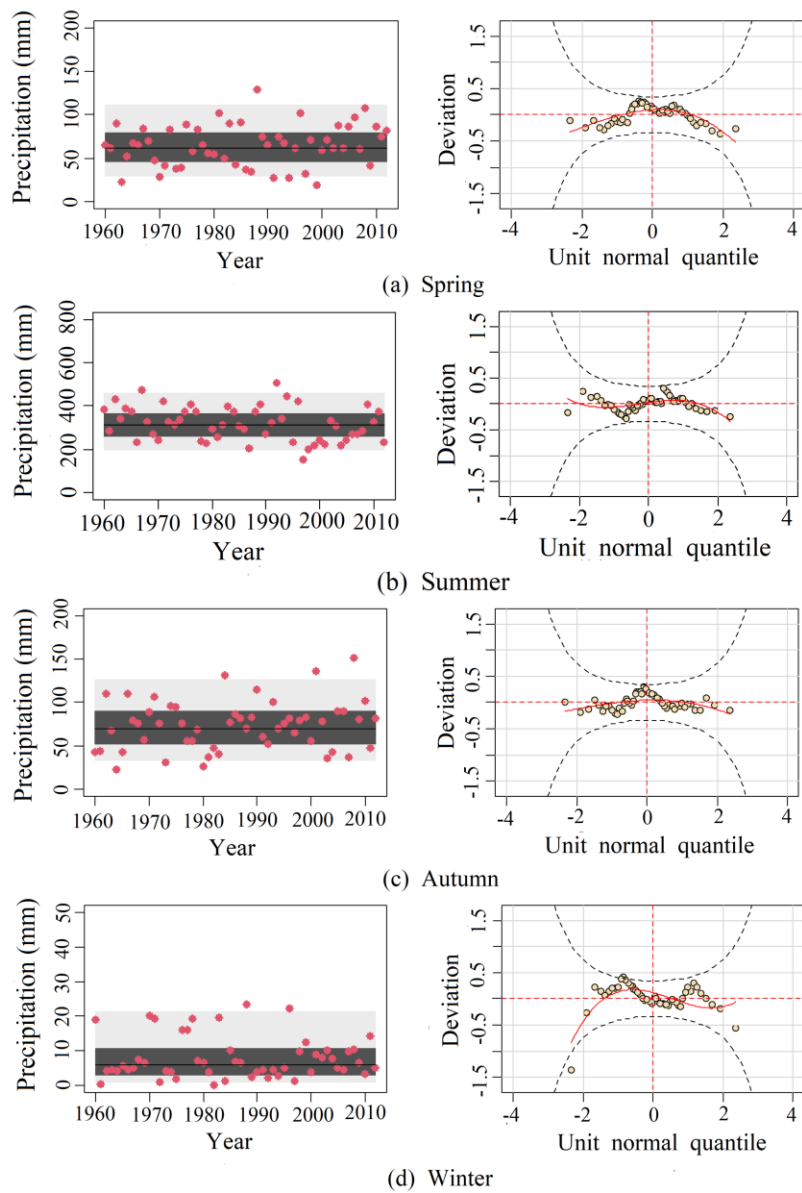
Table 5 Model parameters estimation results in four seasons in the CDS region

Season	Parameters
Spring	$\alpha_t = \exp(4.17 + 0.13AMO_{t-1})$ $\beta_t = \exp(-0.98)$
Summer	$\alpha_t = \exp(5.75 - 0.10AMO_{t-24})$ $\beta_t = \exp(-1.43)$
Autumn	$\alpha_t = \exp(4.29)$ $\beta_t = \exp(0.40)$
Winter	$\alpha_t = \exp(2.04)$ $\beta_t = \exp(-0.20 - 0.49AMO_{t-1} + 0.29AMO_{t-24})$

267 To assess the quality of the fitting, Fig.4 provides the simulation of precipitation from the GAMLSS
 268 framework (Taking the CDS region as an example). As shown in Fig.4, these red dots represent precipitation
 269 observations, light grey areas represent areas between the 5% and 95% centile curves, dark grey areas represent
 270 areas between the 25% and 75% centile curves, and black lines represent median (50%), the black dashed line in
 271 the worm plot of the fitted residuals indicates the 95% confidence interval.

272 It can be seen from Fig.44 that the precipitation data values of the four seasons were basically within the 95%
 273 quantile interval, the deviation values in the worm chart were evenly distributed in the 95% confidence interval,

274 and there was no obvious excess, which indicated that the residual fitting of Gamma distribution meets the
 275 conditions. In general, the temporal behavior associated with the data was significant, the results of the model
 276 (Fig.4) seem to reproduce the behavior of the data, especially to capture the large dispersion characteristics of the
 277 data.



278

Figure 4 Fitting results of four seasons of precipitation series in the CDS region

280 **4.2.2 The simulation of the runoff series**

281 For the simulation of runoff, temperature(T), specific humidity(H), and wind speed(W) were considered as
 282 covariates of the shape and position parameters of the gamma distribution. Some of the model situations
 283 considered are shown in Table 6, and taking the CDS region as an example, the optimal results are listed in Table
 284 7.

Table 6 Different model situations considered for runoff simulation

Model	Parameter	
	α_t	β_t
Mod 1	~1	~1
Mod 2	~1	~ T and H
Mod 3	~ T and H	~1
Mod 4	~1	~ T
Mod 5	~ T	~1
Mod 6	~1	~ H
Mod 7	~ H	~1
Mod 8	~1	~ T, H and W
Mod 9	~ T, H and W	~1

Table 7 AIC, SBC, and GD of the best suitable model of the non-stationary model of runoff in the CDS region

Season	The optimal model	AIC: -70.28
Spring	Mod 9	SBC: -60.43
		GD: -80.27
Summer	Mod 4	AIC:136.19
		SBC:142.10
		GD:130.19
Autumn	Mod 3	AIC: -58.67
		SBC: -50.79
		GD: -66.67
Winter	Mod 3	AIC: -4477
		SBC: -439.89
		GD: -455.77

The results of the estimated model parameters of the runoff in the CDS region as an example were shown in Table 8. As seen in Table 8, the main factors affecting the spring runoff series were temperature, specific humidity, and wind speed, with specific humidity having a greater influence than the other two factors. In summer, temperature was the main factor influencing the runoff series. In autumn and winter, runoff sequences were mainly influenced by temperature and specific humidity.

Table 8 Model parameters estimation results in four seasons of the CDS region

Season	Parameter
Spring	$\alpha_t = \exp(-1.57 - 0.37T_t + 0.54H_t + 0.28W_t)$
	$\beta_t = \exp(-0.42)$
Summer	$\alpha_t = \exp(0.62)$
	$\beta_t = \exp(-0.73 + 0.23T_t)$
Autumn	$\alpha_t = \exp(-1.45 - 0.29T_t + 0.48H_t)$
	$\beta_t = \exp(-0.41)$
Winter	$\alpha_t = \exp(-4.85 - 1.91T_t + 1.34H_t)$
	$\beta_t = \exp(0.48)$

294 The simulation results of the stationary model and non-stationary for runoff in the CDS region are shown in
 295 Fig.5. As can be seen from Fig.5, most of the runoff data values (red points) of the four seasons were located in
 296 the light gray area (5% and 95% centile curves), and the data deviations in the worm plots were evenly
 297 distributed in the 95% confidence interval (between the two black ellipse dotted lines), which show that non-
 298 stationary gamma distribution meet the requirements for the fitting of runoff series. In Fig.5, the non-stationary
 299 model showed the time variation characteristics of the runoff series flexibly. Generally, the non-stationary model
 300 can describe the variability of runoff series accurately. In summary, the non-stationary model with temperature,
 301 humidity, and wind speed were considered as covariates that can capture the time variation characteristics of the
 302 runoff series.

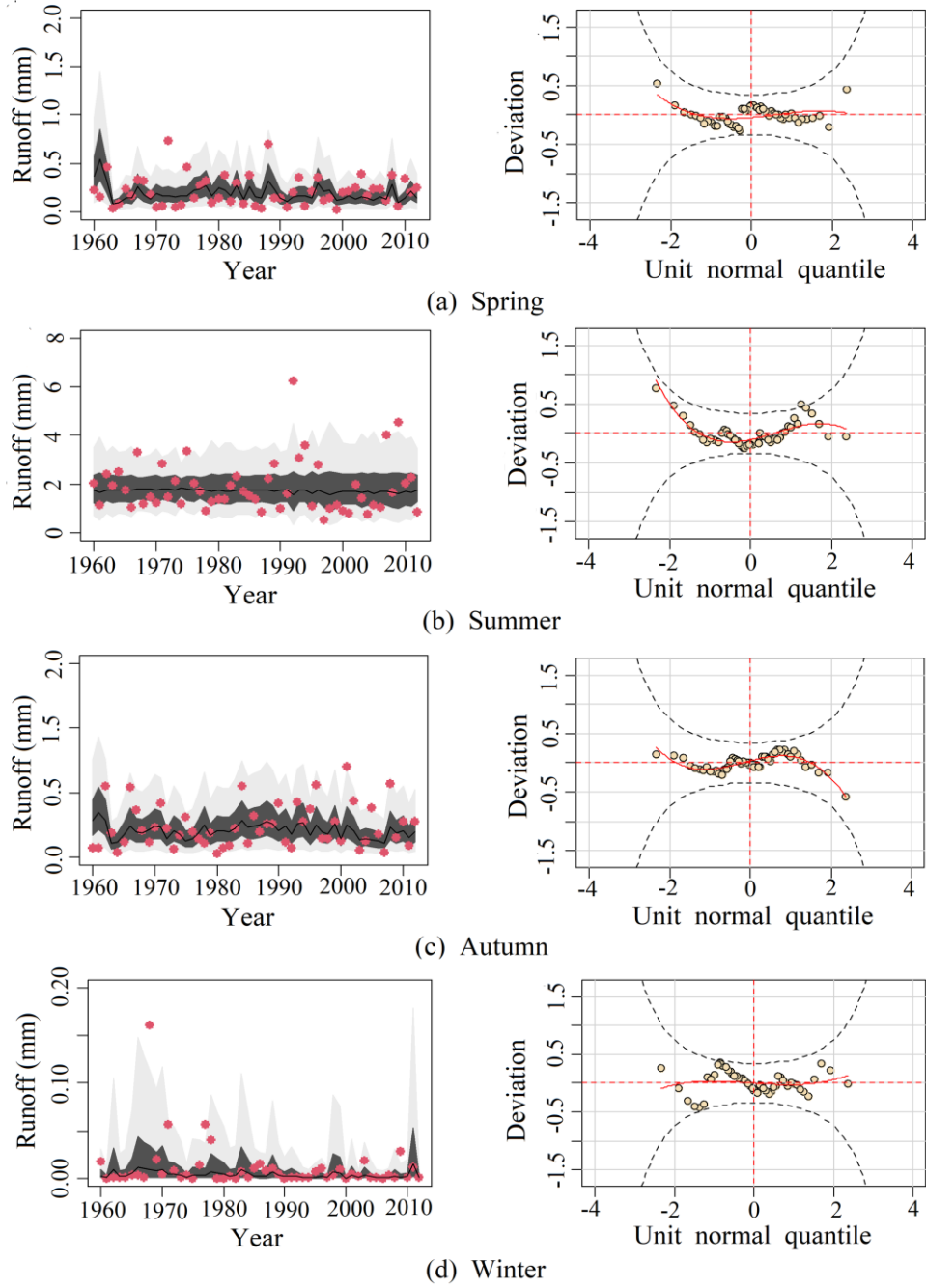
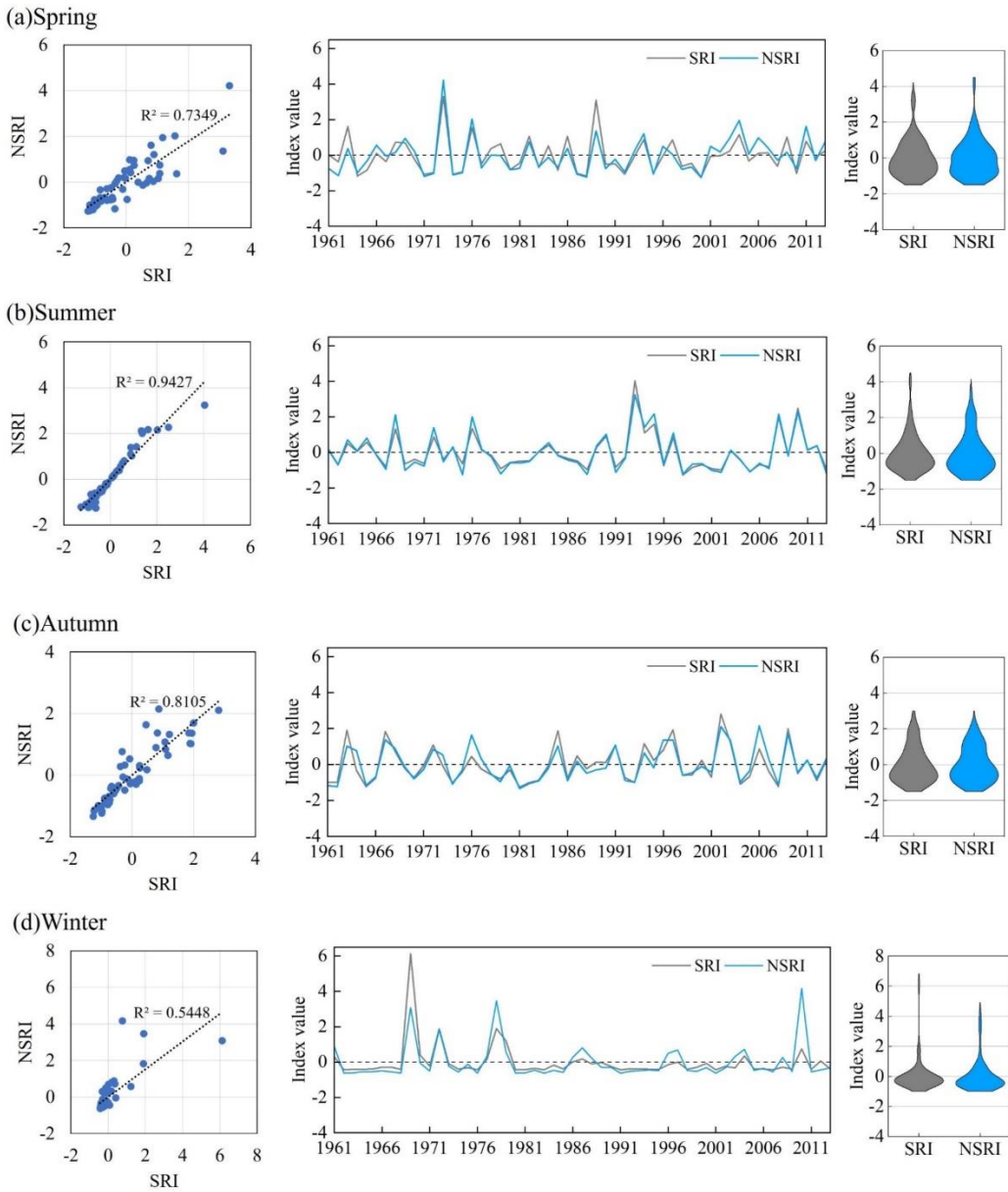


Figure 5 Fitting results of four seasons of runoff series in the CDS region

4.3 Calculation of stationary and non-stationary indices

According to the simulation results of the model in Section 4.2, the non-stationary models have better performance than the stationary models in the simulation of runoff series in all regions. The comparison results of SRI and NSRI in different seasons in CDS are shown in Fig.6. It can be seen that the distribution of two indices is generally similar. Furthermore, the climate factors had different impacts on the index in different seasons, with the smallest impact on summer and the most significant impact on winter.



311

312 **Figure 6 Comparison of SRI and NSRI in different seasons in the CDS region (a: Spring; b: Summer; c:**
 313 **Autumn; d: Winter)**

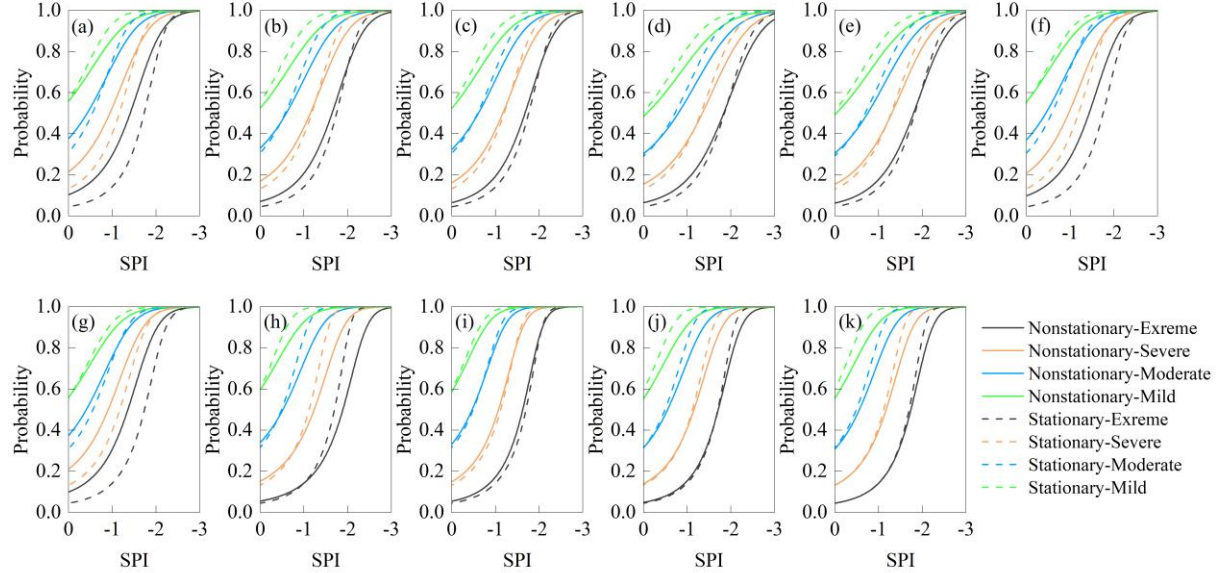
314

4.4 Drought propagation probability

315

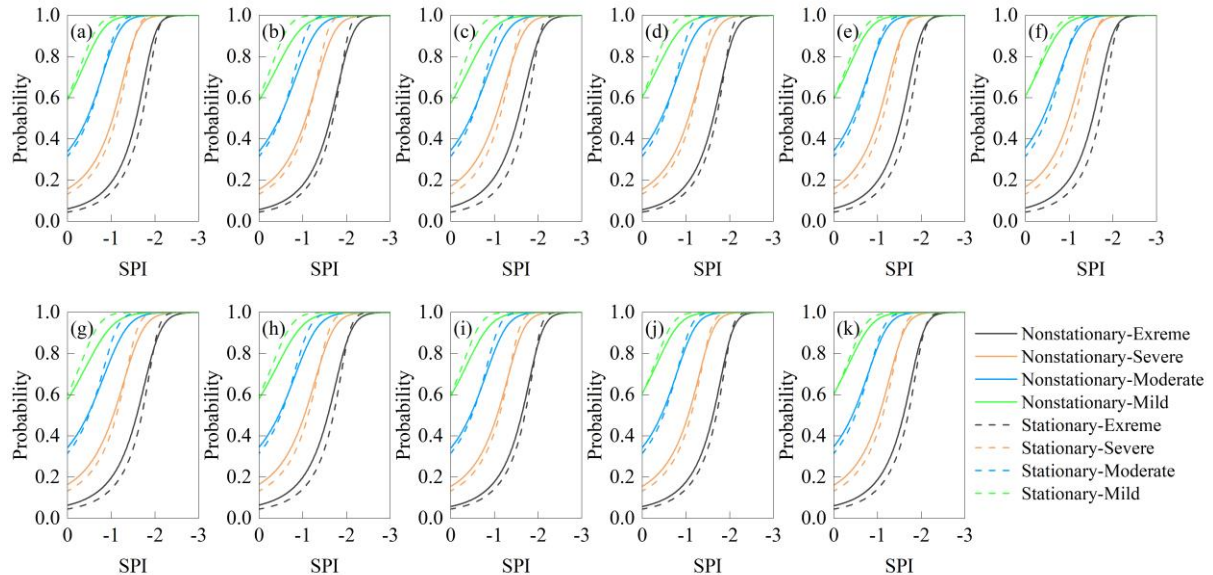
Based on the Copula model, the probabilities of meteorological drought propagation to hydrological
 316 drought can be calculated, and the impact of climate change on drought propagation can be analyzed. The
 317 calculated results in different seasons and different regions were shown in Figs.7-10, where the solid and dashed
 318 lines indicate the calculated results of the non-stationarity model and the stationarity model, respectively, and
 319 black, red, blue, and green represent extreme drought, severe drought, moderate drought, and mild drought,
 320 respectively. According to the analysis results in Figs.7-10, the probabilities of the occurrence of hydrological
 321 drought increased with the decrease of SPI, and as the degree of meteorological drought worsened, it might lead

322 to more severe hydrological drought. In addition, the drought propagation probabilities calculated based on the
 323 non-stationarity model were significantly different from those calculated by the stationarity model, and they also
 324 differ in different seasons and regions.



325
 326 **Figure 7 Probability of drought propagation in spring for each region (a: ZL; b: DL; c: GY; d: FN; e: WC;
 327 f: LH; g: LP; h: CDS; i: CDX; j: PQ; k: KC)**

328 Fig.7 shows the calculated results of drought propagation probabilities in spring in 11 regions. In the
 329 upstream (ZL, DL, GY,) and middle regions (WC, FN, LH, LP, and CDS) of the basin, the drought propagation
 330 probabilities calculated by the non-stationary model were significantly different from those calculated by the
 331 stationary model, while the calculated results were relatively close in the downstream areas such as CDX, PQ
 332 and KC. For the upstream and middle regions, under the same meteorological drought conditions, the
 333 probabilities of severe and extreme hydrological drought calculated based on the non-stationary model were
 334 larger than that of the stationary model, while in the downstream area, the probabilities of hydrological drought
 335 calculated by the stationary model were slightly higher than that of the non-stationary model. According to the
 336 modeling structure of the precipitation and runoff sequence in spring in section 4.2, under the combined
 337 influence of climatic factors AMO, temperature, specific humidity, and wind speed, regional hydrological
 338 drought is more likely to occur. In contrast to the stationary conditions, the increase in temperature may be the
 339 main factor that causes the hydrological drought to become more severe in spring.

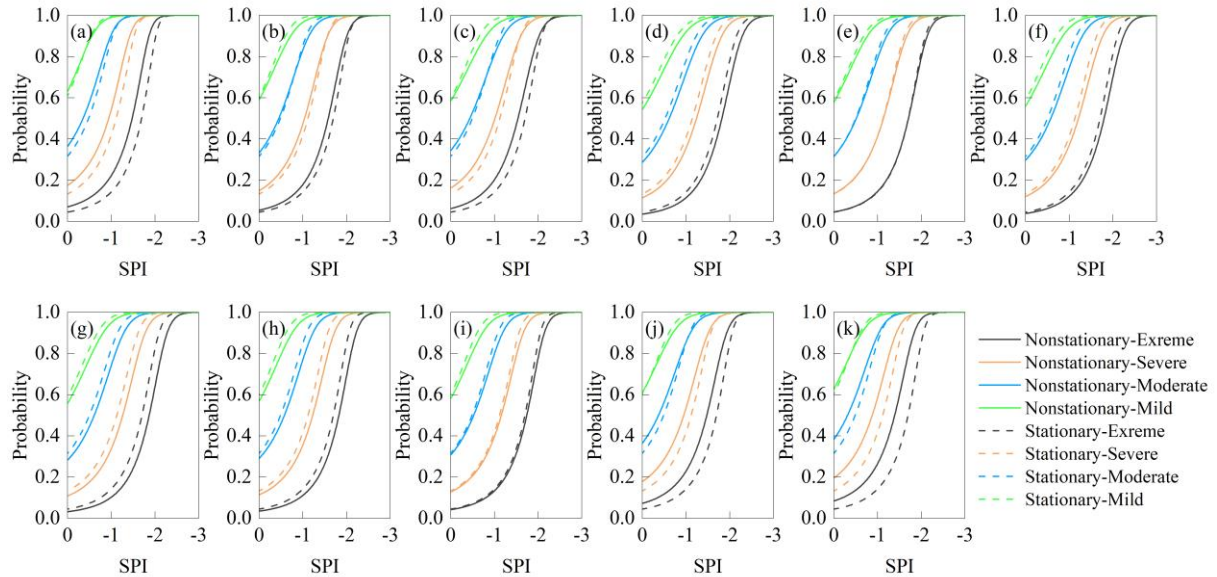


340

341 **Figure 8 Probability of drought propagation in summer for each region (a: ZL; b: DL; c: GY; d: FN; e:**
 342 **WC; f: LH; g: LP; h: CDS; i: CDX; j: PQ; k: KC)**

343 In summer (Fig.8), in each region, the difference between the drought propagation probabilities calculated
 344 by the non-stationary model and the results calculated by the stationary model was not significant, and the
 345 probability of occurrence of severe and extreme hydrological droughts calculated by the non-stationary model
 346 was larger. Taking the ZL region as an example (Fig.8(a)), when climate change was not considered, the
 347 probability of severe hydrological drought and extreme hydrological drought was 0.6 and 0.17, respectively.
 348 Under the influence of the changing environment, the probability of causing severe hydrological drought and
 349 extreme hydrological drought was 0.62 and 0.2 respectively. This means that climate changes had little impact
 350 on drought propagation in the basin during the summer when precipitation was abundant. In contrast to the
 351 stationary conditions, the AMO and temperature may be the main climate reasons for the greater probability of
 352 drought propagation in summer (Zhang et al. 2022).

353 Different from spring and summer, in autumn (Fig.9), The probabilities of occurrence of moderate drought
 354 and more severe hydrological droughts calculated by the non-stationary model were larger than those of the
 355 stationary model in the upstream (ZL, DL, and GY) and downstream regions (CDX, PQ, and KC), which
 356 indicated that the propagation of droughts in the upstream and downstream regions was influenced by climate
 357 change significantly. Temperature and humidity may be the main climate-influencing factors for the significant
 358 increase of the drought propagation probability in the upstream and downstream areas. Unlike the upstream and
 359 downstream areas, these climatic factors may not be the main cause of the propagation of drought in the
 360 midstream region (WC, FN, LH, LP, and CDS).



361

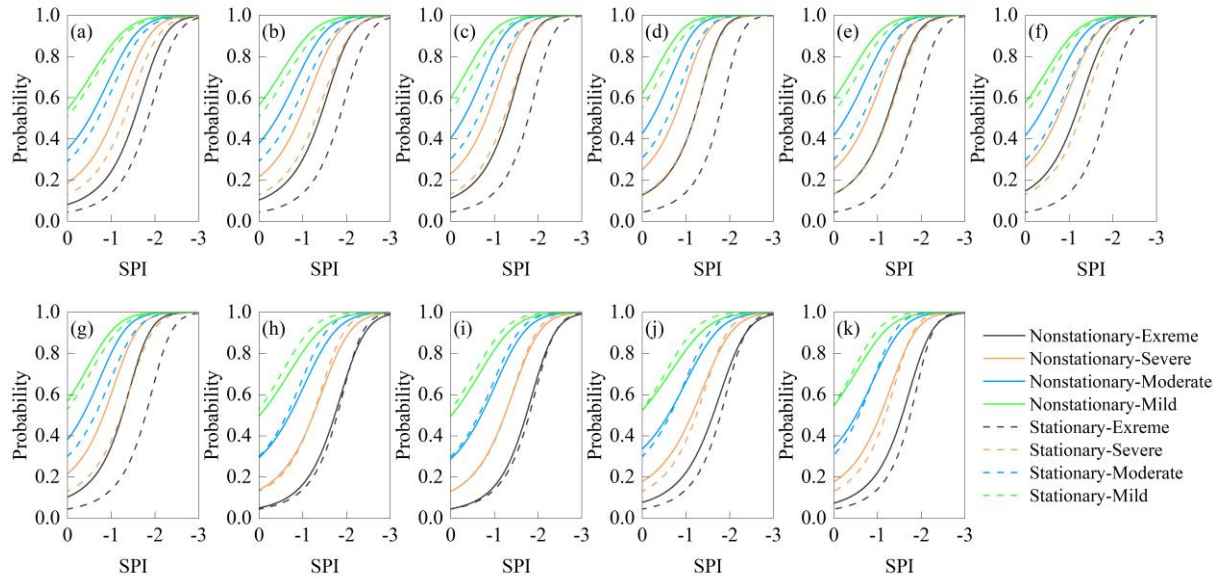
362

Figure 9 Probability of drought propagation in autumn for each region (a: ZL; b: DL; c: GY; d: FN; e: WC; f: LH; g: LP; h: CDS; i: CDX; j: PQ; k: KC)

363

364

In winter (Fig.10), the probabilities of occurrence of moderate and more severe hydrological droughts in the upstream and midstream regions calculated based on the non-stationary model were significantly larger than those calculated by the stationary model. Taking the WC station as an example, when climate change was not considered, the probabilities of occurrence of moderate, severe, and extreme hydrological droughts under moderate meteorological drought conditions were about 0.8, 0.6, and 0.4, respectively, while under the influence of environmental change, the probabilities of moderate, severe and extreme hydrological droughts were about 0.9, 0.8 and 0.6, respectively. In most of the downstream areas, the difference between the calculation results of the two models was relatively small. Under the combined influence of AMO, temperature, wind speed, and specific humidity, the probabilities of drought propagation are increased. In upstream, the decrease in wind speed may be the main climate factors affecting the occurrence of severe drought, and the increase in temperature and the decrease in specific humidity may be the main climate factors affecting the occurrence of severe drought in midstream regions. In downstream areas, these climatic factors may not be the main influences on drought propagation.



377

378
379

Figure 10 Probability of drought propagation in winter for each region (a: ZL; b: DL; c: GY; d: FN; e: WC; f: LH; g: LP; h: CDS; i: CDX; j: PQ; k: KC)

380
381
382
383
384
385
386
387
388
389
390
391
392
393
394
395
396
397

Comparing the four seasons, the probabilities of occurrence of moderate and more severe droughts were the lowest in spring, but the highest in winter, this phenomenon was significant under non-stationarity conditions. Taking the FN region as an example (Fig.7(d)- Fig.10(d)), the probabilities of moderate meteorological drought propagating as moderate, severe, and extreme hydrological drought in spring under non-stationarity conditions were close to 0.6, 0.4, and 0.15, respectively, while in winter, the probabilities of propagating as moderate, severe and extreme hydrological drought under the same meteorological drought conditions were close to 0.9, 0.7 and 0.4, respectively. The reasons for the differences in the probabilities of drought propagation under stationary and non-stationary conditions are complex. On the one hand, non-stationary models capture changes caused by interannual variability, and on the other hand, they are affected by AMO, temperature, wind speed, and relative humidity. There may be some differences in the effects of various meteorological factors on drought in different seasons. From the results in Section 4.2, the drought propagation is affected by the combined effects of AMO, temperature, wind speed, and relative humidity in spring, with relative humidity as the main influencing factor. In summer, drought propagation is mainly influenced by AMO and temperature. In the fall, it is influenced by temperature and relative humidity, with relative humidity being the main influencing factor. In winter, it is influenced by a combination of AMO, temperature, and relative humidity, with temperature being the most important influencing factor. Comparing the four seasons, meteorological factors have the most serious effect on winter drought. In addition, there are some differences in the effects of meteorological factors on drought in different regions. Temperatures show a significant upward trend, which may mean that extreme runoff

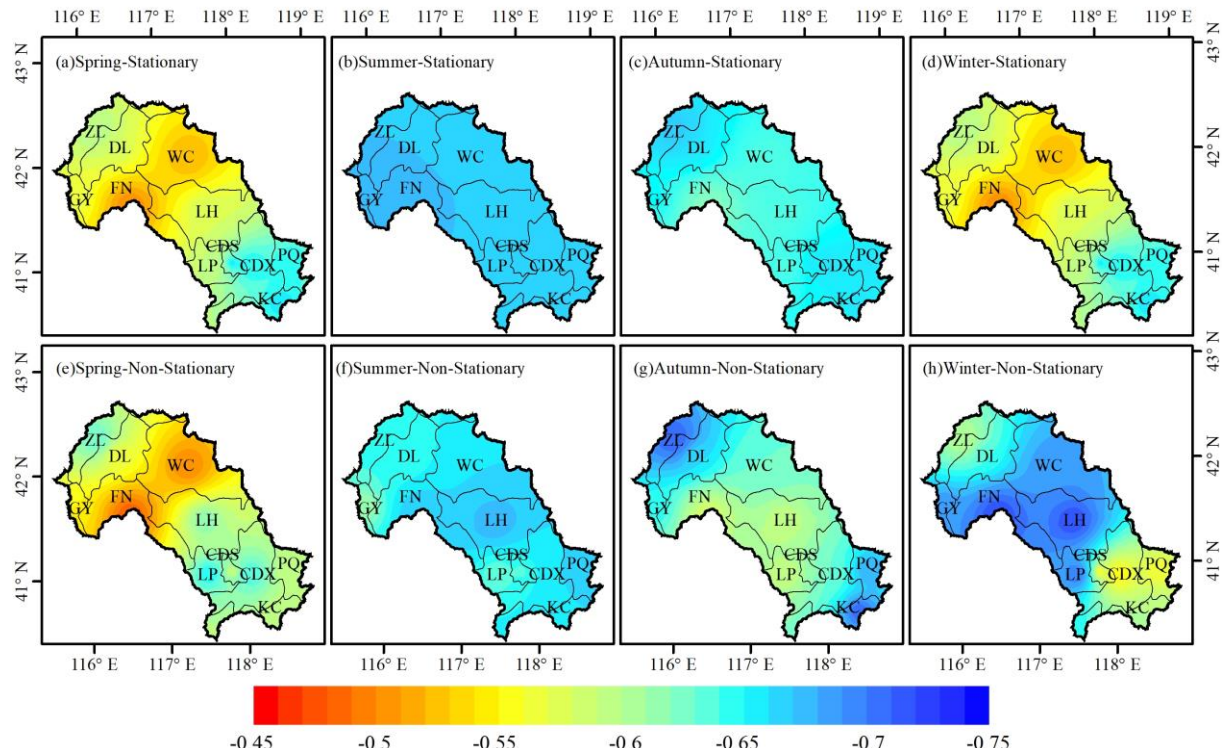
398 events will be more frequent. During the dry season, high temperatures increase evapotranspiration from surface
399 water bodies, vegetation, etc., resulting in reduced runoff and lower soil moisture content will increase the risk of
400 hydrological drought (Huang et al. 2017; Guo et al. 2021). Changes in humidity affect the efficiency of
401 evapotranspiration, and higher humidity will reduce the transfer of water from the surface and plants to the
402 atmosphere, limiting the development of drought. However, this effect may be limited by increased evaporation
403 from increasing temperatures.

404 **4.5 Drought propagation threshold**

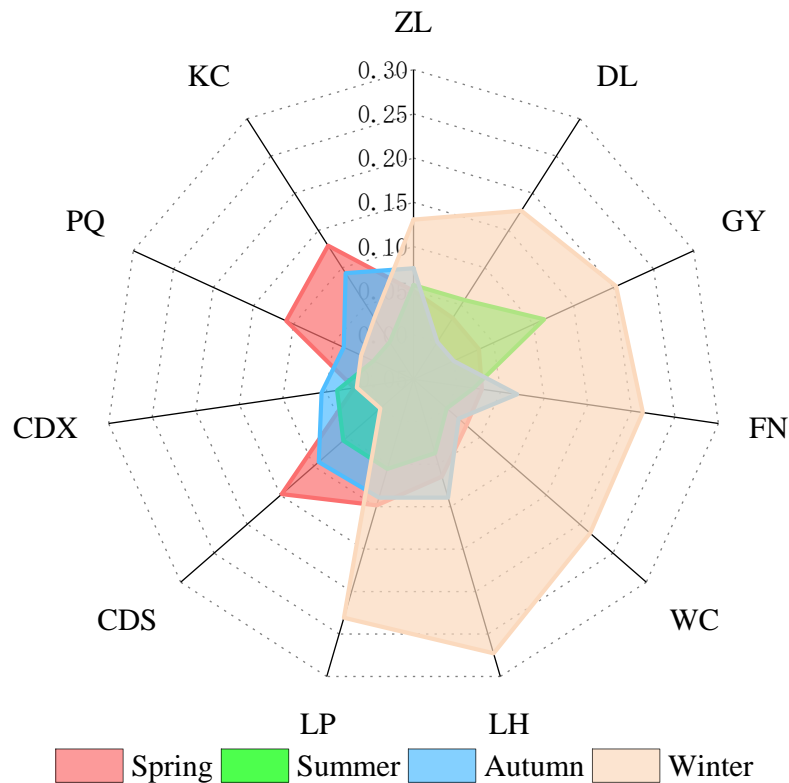
405 Based on the Copula model, the thresholds that trigger hydrological droughts under stationary and non-
406 stationary conditions (i.e., the propagation thresholds for drought) can be calculated, the results are shown in Fig.
407 11. The change rate of the meteorological drought to hydrological drought propagation thresholds are shown in
408 Figure 12 As can be seen from Figs.11 and 12, there were obvious regional and seasonal characteristics of
409 drought propagation thresholds. In this paper, the higher the drought propagation thresholds, the more likely
410 hydrological drought is to be triggered.

411 In spring (Fig.11(a)), comparing the results of calculations based on the stationary model and the non-
412 stationary model, the drought propagation thresholds were the smallest in FN, WC region, and the highest values
413 occurred in the downstream region (CDS, CDX, PQ, KC) under the stationary condition. The distribution of
414 drought propagation thresholds under non-stationary conditions was similar to that under stationary conditions.
415 In addition, compared with the stationary condition, the drought propagation thresholds were higher in most
416 regions under non-stationary condition. It indicated that hydrological droughts were more difficult to be
417 triggered in most regions under the influence of climatic factors such as temperature, specific humidity, wind
418 speed, and AMO. In summer (Fig. 11(b)), There was no significant difference in drought propagation thresholds
419 in all regions under stationary conditions and non-stationary conditions. In autumn (Fig. 11(c)), the drought
420 propagation thresholds in the river basin were close to that in summer. Under stationary conditions, the drought
421 propagation thresholds were close to -0.55 in most regions. Comparing stationary conditions, the drought
422 propagation thresholds increased in ZL, PQ, and KC, while decreasing in middle-stream areas (FN, WC, LH, LP,
423 CDS, CDX) under non-stationary conditions. In winter (Fig. 11(d)), there were significant differences in regional
424 drought propagation thresholds between stationary and non-stationary conditions. Under stationary conditions,
425 the drought propagation thresholds of the basin were relatively lower than those in spring, summer, and autumn,
426 with values ranging from -0.70 to -0.65. Under non-stationary conditions, the drought propagation thresholds

427 increased generally, especially in the midstream region. From Fig. 12, it can be seen that drought propagation
 428 thresholds were most affected by large-scale climate factors and meteorological factors in winter, with a rate of
 429 change greater than 10% or even 20% in most regions, followed by spring, with the least change in the summer
 430 and autumn seasons. It indicated that hydrological drought was more likely to occur during winter due to climate
 431 factors.



432
 433 **Figure 11 Drought propagation thresholds in different seasons under stationary and non-stationary
 434 conditions**



452 the relationships between the propagation thresholds and the factors were explored for each region. As shown in
 453 Table 9` , these factors may be one of the reasons for the spatial differences in drought propagation thresholds.
 454 Evapotranspiration and shallow soil moisture are dominant among these factors, followed by the effects of slope
 455 and vegetation on drought propagation. The drought resistance of the watershed decreases when the slope
 456 increases and the water storage capacity decreases, and meteorological droughts are more likely to trigger
 457 hydrologic droughts. Evapotranspiration is a key part of the water cycle and directly reflects the exchange of
 458 water between soil, vegetation, and the atmosphere. There is a positive correlation between evapotranspiration
 459 and drought propagation thresholds, and an increase in evapotranspiration leads to a decrease in surface water
 460 resources, which may increase the risk of drought propagation(Guo et al. 2020; Yao et al. 2022). Soil moisture
 461 content may also be one of the factors causing spatial differences in drought propagation thresholds, with
 462 shallow soil having a greater impact on drought propagation than deep soil. Vegetation cover also affects drought
 463 propagation, and more vegetation can increase water retention in a watershed and improve its drought resistance.
 464 However, when meteorological drought is severe, vegetation in a water-starved condition will consume more
 465 water through transpiration, accelerating the onset of drought.

466 **Table 9 The characteristics of the study area, including slope, evapotranspiration(E), soil moisture content**
 467 **(0-10 cm underground) (SMC0-10cm), soil moisture content (10-40 cm underground) (SMC10-40cm), soil**
 468 **moisture content (40-100 cm underground) (SMC40-100cm), soil moisture content (100-200 cm**
 469 **underground) (SMC100-200cm), Lead area index (LAI)**

Region	Slope	E(mm)	SMC0-	SMC10-	SMC40-	SMC100-	LAI
			10 cm	40 cm	100 cm	200 cm	
ZL	2.30	84.76	42.35	130.30	183.53	522.55	0.50
DL	3.60	88.79	42.67	129.60	180.51	524.61	0.50
GY	2.36	90.27	43.43	132.57	184.80	531.07	0.56
FN	10.35	96.61	44.19	136.50	196.74	523.87	0.86
WC	10.06	95.28	42.38	122.27	171.65	514.83	1.03
LH	12.64	103.76	46.84	143.74	216.09	456.18	1.21
LP	12.48	110.20	48.25	149.69	230.37	477.93	1.08
CDS	10.27	112.99	55.99	157.92	236.12	612.83	0.81
CDX	13.04	113.28	45.93	143.71	231.90	394.67	1.31
PQ	11.59	114.56	45.30	135.91	209.45	516.40	1.02

KC	14.56	117.83	45.81	139.27	222.59	465.23	1.24
Pearson for PT	0.34	0.71	0.48	0.50	0.66	-0.09	0.23

470 **6. Conclusions**

471 Many studies have pointed out that climate change and human activities significantly impact the occurrence
 472 of drought in the Luanhe River basin. In this paper, meteorological drought and hydrological drought were
 473 characterized by the SPI and SRI respectively. The drought propagation probabilities and thresholds in all
 474 seasons were calculated based on the non-stationary drought index constructed by the GAMLSS model and the
 475 Copula function, the influence of climate change and watershed characteristics on drought propagation was
 476 analyzed. The following conclusions can be drawn.

477 (1) AMO-1 and AMO-24 have a significant impact on the precipitation series in the Luanhe River basin.
 478 The temperature, wind speed, and specific humidity were considered as the main influencing climate factors of
 479 the runoff series.

480 (2) Based on the GAMLSS framework, both the stationary model and non-stationary model have a good
 481 fitting effect on the precipitation and runoff series of the basin, but overall, the non-stationary model can capture
 482 the time variation characteristics of these series more accurately.

483 (3) For most regions, the probabilities of drought propagation under non-stationary conditions were greater
 484 than that under stationarity conditions. Compared to summer and autumn, spring and winter were more prone to
 485 hydrological drought and may experience more severe hydrological drought.

486 (4) With regard to the drought propagation thresholds, non-stationary conditions were more likely to trigger
 487 hydrological drought than stationary conditions, this phenomenon was particularly evident in the midstream and
 488 upstream regions in winter, with drought propagation thresholds increasing by 0.1-0.2 under non-stationary
 489 conditions compared to stationary conditions. The increase of temperature may be the key factors contributing to
 490 the occurrence of hydrological drought in the basin.

491 (5) Watershed characteristics were important factors in the spatial differences of drought propagation
 492 characteristics, including vegetation cover and so on. Among them, there was a high correlation (the absolute
 493 value of correlation coefficient > 0.5) between evapotranspiration, soil moisture content (10-40 cm underground,
 494 40-100 cm underground) and drought propagation characteristics.

495 **Limitation:** There are many driving factors for the propagation of drought, and climate change and human
496 activities are important factors among them. In this paper, we analyzed the effects of temperature, specific
497 humidity, wind speed, and large-scale climate factors on drought and its propagation. However, there are
498 numerous and complex factors that affect drought propagation, and different factors interact with each other. It is
499 necessary to consider the interaction of topography, vegetation coverage, human activities, and climate change,
500 so as to provide more effective support for drought resistance and control measures.

501 **Competing interests:**

502 The authors declare that they have no conflict of interest.

503 **Author Contributions:**

504 Min Li (First Author and Corresponding Author): Conceptualization, Methodology, Software, Investigation,
505 Formal Analysis, Writing-Original Draft;
506 Zilong Feng: Data Curation, Writing-Original Draft, Writing-Review & Editing;
507 Mingfeng Zhang: Visualization, Investigation;
508 Lijie Shi: Supervision, Validation;
509 Yuhang Yao: Investigation, Data Curation.

510 **Acknowledgements.**

511 We are grateful to the the National Oceanic and Atmospheric Administration
512 (<http://www.esrl.noaa.gov/psd/data/climateindices>) for providing the large climate indices data, and grateful to
513 the GLDAS (https://disc.gsfc.nasa.gov/datasets/GLDAS_NOAH10_M_2.0/) for providing the average monthly
514 precipitation, temperature, wind speed, specific humidity, evapotranspiration, soil water content datasets and the
515 runoff datasets. The data and materials of the research are available.

516 **Funding Information**

517 This work was supported by the State Key Laboratory of Hydraulic Engineering Intelligent Construction and
518 Operation (No. HESS-2206), and the Open Fund of Key Laboratory of Flood & Drought Disaster Defense, the
519 Ministry of Water Resources (KYFB202307260034).

520 **References**

521 Apurv T and Cai X. Drought Propagation in Contiguous U.S. Watersheds: A Process-Based Understanding of the

522 Role of Climate and Watershed Properties, Water Resources Research, 56, e2020WR027755.
523 <https://doi.org/10.1029/2020WR027755>, 2020.

524 Bhardwaj K, Shah D, Aadhar S and Mishra V. Propagation of Meteorological to Hydrological Droughts in India,
525 Journal of Geophysical Research: Atmospheres, 125, e2020JD033455. <https://doi.org/10.1029/2020JD033455>,
526 2020.

527 Chen X, Li F-w, Wang Y-x, Feng P and Yang R-z. Evolution properties between meteorological, agricultural and
528 hydrological droughts and their related driving factors in the Luanhe River basin, China, Hydrology Research,
529 50, 1096-1119. <https://doi.org/10.2166/nh.2019.141> 2019.

530 Chen X, Han R, Feng P and Wang Y. Combined effects of predicted climate and land use changes on future
531 hydrological droughts in the Luanhe River basin, China, Natural Hazards, 110, 1305-1337.
532 <https://doi.org/10.1007/s11069-021-04992-3>, 2022.

533 Cheng X, Xu Y, Chen J and Liu Q. The Impact of Climatic Conditions, Human Activities, and Catchment
534 Characteristics on the Propagation From Meteorological to Agricultural and Hydrological Droughts in China,
535 Journal of Geophysical Research: Atmospheres, 128, e2023JD039735. <https://doi.org/10.1029/2023JD039735>,
536 2023.

537 Das S, Das J and Umamahesh N V. Investigating the propagation of droughts under the influence of large-scale
538 climate indices in India, Journal of Hydrology, 610, 127900. <https://doi.org/10.1016/j.jhydrol.2022.127900>, 2022.

539 Dehghani M, Saghafian B and Zargar M. Probabilistic hydrological drought index forecasting based on
540 meteorological drought index using Archimedean copulas, Hydrology Research, 50, 1230-1250.
541 <https://doi.org/10.2166/nh.2019.051>, 2019.

542 Ding Y, Xu J, Wang X, Cai H, Zhou Z, Sun Y and Shi H. Propagation of meteorological to hydrological drought
543 for different climate regions in China, Journal of Environmental Management, 283, 111980.
544 <https://doi.org/10.1016/j.jenvman.2021.111980>, 2021.

545 Gao Y, Niu Y, Sun W, Liu K, Liu X, Zhao N, Yue Y, Wu H, Meng F, Wang J, Wang X and Liu Q. Climate factors
546 driven typhus group rickettsiosis incidence dynamics in Xishuangbanna Dai autonomous prefecture of Yunnan
547 province in China, 2005–2017, Environmental Health, 19, 3. <https://doi.org/10.1186/s12940-019-0558-3>, 2020.

548 Guo Y, Huang S, Huang Q, Leng G, Fang W, Wang L and Wang H. Propagation thresholds of meteorological
549 drought for triggering hydrological drought at various levels, Science of The Total Environment, 712, 136502.
550 <https://doi.org/10.1016/j.scitotenv.2020.136502>, 2020.

551 Guo Y, Huang Q, Huang S, Leng G, Zheng X, Fang W, Deng M and Song S. Elucidating the effects of mega

552 reservoir on watershed drought tolerance based on a drought propagation analytical method, Journal of
553 Hydrology, 598, 125738. <https://doi.org/10.1016/j.jhydrol.2020.125738>, 2021.

554 Han Z, Huang S, Huang Q, Leng G, Wang H, Bai Q, Zhao J, Ma L, Wang L and Du M. Propagation dynamics
555 from meteorological to groundwater drought and their possible influence factors, Journal of Hydrology, 578,
556 124102. <https://doi.org/10.1016/j.jhydrol.2019.124102>, 2019.

557 Han Z, Huang S, Zhao J, Leng G, Huang Q, Zhang H and Li Z. Long-chain propagation pathways from
558 meteorological to hydrological, agricultural and groundwater drought and their dynamics in China, Journal of
559 Hydrology, 625, 130131. <https://doi.org/10.1016/j.jhydrol.2023.130131>, 2023.

560 Hao Y, Liu Q, Li C, Kharel G, An L, Stebler E, Zhong Y and Zou C B. Interactive Effect of Meteorological
561 Drought and Vegetation Types on Root Zone Soil Moisture and Runoff in Rangeland Watersheds, Water, 11,
562 <https://doi.org/10.3390/w11112357>, 2019.

563 Huang S, Li P, Huang Q, Leng G, Hou B and Ma L. The propagation from meteorological to hydrological
564 drought and its potential influence factors, Journal of Hydrology, 547, 184-195.
565 <https://doi.org/10.1016/j.jhydrol.2017.01.041>, 2017.

566 Jehanzaib M, Sattar M N, Lee J-H and Kim T-W. Investigating effect of climate change on drought propagation
567 from meteorological to hydrological drought using multi-model ensemble projections, Stochastic Environmental
568 Research and Risk Assessment, 34, 7-21. <https://doi.org/10.1007/s00477-019-01760-5>, 2020.

569 Jehanzaib M, Ali S, Kim M J and Kim T-W. Modeling hydrological non-stationarity to analyze environmental
570 impacts on drought propagation, Atmospheric Research, 286, 106699.
571 <https://doi.org/10.1016/j.atmosres.2023.106699>, 2023.

572 Kang E, Meng H and Li X. Time series prediction of EMD-ELM gas emission amount base on Pearson
573 correlation test, Modern Electronics Technique, 45(05), 134-138. <https://doi.org/10.16652/j.issn.1004-373x.2022.05.023>, 2022. (in Chinese)

575 Kolachian R and Saghafian B. Hydrological drought class early warning using support vector machines and
576 rough sets, Environmental Earth Sciences, 80, 390. <https://doi.org/10.1007/s12665-021-09536-3>, 2021.

577 Kumar S, Kumar P, Barat A, Sinha A K, Sarthi P P, Ranjan P and Singh K K. Characteristics of Observed
578 Meteorological Drought and its Linkage with Low-Level Easterly Wind Over India, Pure and Applied
579 Geophysics, 176, 2679-2696. <https://doi.org/10.1007/s00024-019-02118-2>, 2019.

580 Le M H, Perez G C, Solomatine D and Nguyen L B. Meteorological Drought Forecasting Based on Climate
581 Signals Using Artificial Neural Network – A Case Study in Khanhhoa Province Vietnam, Procedia Engineering,

582 154, 1169-1175. <https://doi.org/10.1016/j.proeng.2016.07.528>, 2016.

583 Li J and Zhou S. Quantifying the contribution of climate- and human-induced runoff decrease in the Luanhe
584 river basin, China, *Journal of Water and Climate Change*, 7, 430-442. <https://doi.org/10.2166/wcc.2015.041>,
585 2016.

586 Li J Z, Wang Y X, Li S F and Hu R. A Nonstationary Standardized Precipitation Index incorporating climate
587 indices as covariates, *Journal of Geophysical Research: Atmospheres*, 120, 12,082-12,095.
588 <https://doi.org/10.1002/2015JD023920>, 2015.

589 Li M, Zhang T and Feng P. A nonstationary runoff frequency analysis for future climate change and its
590 uncertainties, *Hydrological Processes*, 33, 2759-2771. <https://doi.org/10.1002/hyp.13526>, 2019a.

591 Li M, Zhang T, Li J and Feng P. Hydrological Drought Forecasting Incorporating Climatic and Human-Induced
592 Indices, *Weather and Forecasting*, 34, 1365-1376. <https://doi.org/10.1175/WAF-D-19-0029.1>, 2019b.

593 Li M, Zhang T and Feng P. Bivariate frequency analysis of seasonal runoff series under future climate change,
594 *Hydrological Sciences Journal*, 65, 2439-2452. <https://doi.org/10.1080/02626667.2020.1817927>, 2020.

595 Li M, Zhang M, Cao R, Sun Y and Deng X. Hydrological drought forecasting under a changing environment in
596 the Luanhe River basin, *Nat. Hazards Earth Syst. Sci.*, 23, 1453-1464. <https://doi.org/10.5194/nhess-23-1453-2023>, 2023.

598 Li M, Feng Z, Zhang M and Yao Y. Influence of large-scale climate indices and regional meteorological elements
599 on drought characteristics in the Luanhe River Basin, *Atmospheric Research*, 300, 107219.
600 <https://doi.org/10.1016/j.atmosres.2024.107219>, 2024.

601 Lilhake R, Pokorný S, Déry S J, Stadnyk T A and Koenig K A. Sensitivity analysis and uncertainty assessment in
602 water budgets simulated by the variable infiltration capacity model for Canadian subarctic watersheds,
603 *Hydrological Process*, 34, 2057-2075. <https://doi.org/10.1002/hyp.13711>, 2020.

604 Liu Q, Yang Y, Liang L, Jun H, Yan D, Wang X, Li C and Sun T. Thresholds for triggering the propagation of
605 meteorological drought to hydrological drought in water-limited regions of China, *Science of The Total
606 Environment*, 876, 162771. <https://doi.org/10.1016/j.scitotenv.2023.162771>, 2023.

607 Liu Y, Huang S, Guo Y, Li Z and Huang Q. Propagation threshold of meteorological drought to different levels
608 of hydrological drought. A case study of Qinhe River basin, *Journal of Hydroelectric Engineering*, 41, 9-19.
609 <https://doi.org/10.11660/slfdb.20220202>, 2022. (in Chinese)

610 Mahmoudi P, Rigi A and Miri Kamak M. Evaluating the sensitivity of precipitation-based drought indices to
611 different lengths of record, *Journal of Hydrology*, 579, 124181. <https://doi.org/10.1016/j.jhydrol.2019.124181>,

612 2019.

613 Mann H B. Nonparametric tests against trend., *Econometrica: Journal of the Econometric Society*, 13(3), 245-
614 259. 1945.

615 McKee T B, Doesken N J and Kleist J. The relationship of drought frequency and duration to time scale,
616 Proceedings of the 8th Conference on Applied Climatology, 17, pp, 179–183. 1993.

617 Pandey V, Srivastava P K, Mall R K, Munoz-Arriola F and Han D. Multi-satellite precipitation products for
618 meteorological drought assessment and forecasting in Central India, *Geocarto International*, 37, 1899-1918.
619 <https://doi.org/10.1080/10106049.2020.1801862>, 2022.

620 Peña-Gallardo M, Vicente-Serrano S M, Hannaford J, Lorenzo-Lacruz J, Svoboda M, Domínguez-Castro F,
621 Maneta M, Tomas-Burguera M and Kenawy A E. Complex influences of meteorological drought time-scales on
622 hydrological droughts in natural basins of the contiguous United States, *Journal of Hydrology*, 568, 611-625.
623 <https://doi.org/10.1016/j.jhydrol.2018.11.026>, 2019.

624 Rigby R A and Stasinopoulos D M. Generalized Additive Models for Location, Scale and Shape, *Journal of the
625 Royal Statistical Society Series C: Applied Statistics*, 54, 507-554. [https://doi.org/10.1111/j.1467-9876.2005.00510.x](https://doi.org/10.1111/j.1467-
626 9876.2005.00510.x), 2005.

627 Sattar M N, Jehanzaib M, Kim J E, Kwon H-H and Kim T-W. Application of the Hidden Markov Bayesian
628 Classifier and Propagation Concept for Probabilistic Assessment of Meteorological and Hydrological Droughts
629 in South Korea, *Atmosphere*, 11, 1000. <https://doi.org/10.3390/atmos11091000>, 2020.

630 Shao S, Zhang H, Singh V P, Ding H, Zhang J and Wu Y. Nonstationary analysis of hydrological drought index
631 in a coupled human-water system: Application of the GAMLSS with meteorological and anthropogenic
632 covariates in the Wuding River basin, China, *Journal of Hydrology*, 608, 127692.
633 <https://doi.org/10.1016/j.jhydrol.2022.127692>, 2022.

634 Shukla S and Wood A W. Use of a standardized runoff index for characterizing hydrologic drought, *Geophysical
635 Research Letters*, 35, <https://doi.org/10.1029/2007GL032487>, 2008.

636 Tao L, Ryu D, Western A and Boyd D. A New Drought Index for Soil Moisture Monitoring Based on MPDI-
637 NDVI Trapezoid Space Using MODIS Data, *Remote Sensing*, 13, 122. <https://doi.org/10.3390/rs13010122>, 2021.

638 Vicente-Serrano S M, Beguería S and López-Moreno J I. A Multiscalar Drought Index Sensitive to Global
639 Warming: The Standardized Precipitation Evapotranspiration Index, *Journal of Climate*, 23, 1696-1718.
640 <https://doi.org/10.1175/2009JCLI2909.1>, 2010.

641 Vorobevskii I, Kronenberg R and Bernhofer C. Linking different drought types in a small catchment from a

642 statistical perspective – Case study of the Wernersbach catchment, Germany, Journal of Hydrology X, 15,
643 100122. <https://doi.org/10.1016/j.hydroa.2022.100122>, 2022.

644 Wang F, Lai H, Li Y, Feng K, Zhang Z, Tian Q, Zhu X and Yang H. Dynamic variation of meteorological
645 drought and its relationships with agricultural drought across China, Agricultural Water Management, 261,
646 107301. <https://doi.org/10.1016/j.agwat.2021.107301>, 2022.

647 Wang H, Zhu Y, Qin T and Zhang X. Study on the propagation probability characteristics and prediction model
648 of meteorological drought to hydrological drought in basin based on copula function, Frontiers in Earth Science,
649 10, <https://doi.org/10.3389/feart.2022.961871>, 2022.

650 Wang Y, Li J, Feng P and Chen F. Effects of large-scale climate patterns and human activities on hydrological
651 drought: a case study in the Luanhe River basin, China, Natural Hazards, 76, 1687-1710.
652 <https://doi.org/10.1007/s11069-014-1564-y>, 2015.

653 Wang Y, Li J, Feng P and Hu R. A Time-Dependent Drought Index for Non-Stationary Precipitation Series,
654 Water Resources Management, 29, 5631-5647. 10.1007/s11269-015-1138-0, 2015.

655 Wang Y, Li J, Feng P and Hu R. Analysis of drought characteristics over Luanhe River basin using the joint
656 deficit index, Journal of Water and Climate Change, 7, 340-352. <https://doi.org/10.2166/wcc.2015.108>, 2016.

657 Wang Y, Zhang T, Chen X, Li J and Feng P. Spatial and temporal characteristics of droughts in Luanhe River
658 basin, China, Theoretical and Applied Climatology, 131, 1369-1385. <https://doi.org/10.1007/s00704-017-2059-z>,
659 2018.

660 Wang Y, Duan L, Liu T, Li J and Feng P. A Non-stationary Standardized Streamflow Index for hydrological
661 drought using climate and human-induced indices as covariates, Science of The Total Environment, 699, 134278.
662 <https://doi.org/10.1016/j.scitotenv.2019.134278>, 2020.

663 Wang Y, Peng T, He Y, Singh V P, Lin Q, Dong X, Fan T, Liu J, Guo J and Wang G. Attribution analysis of non-
664 stationary hydrological drought using the GAMLSS framework and an improved SWAT model, Journal of
665 Hydrology, 627, 130420. <https://doi.org/10.1016/j.jhydrol.2023.130420>, 2023.

666 Wossenyeleh B K, Worku K A, Verbeiren B and Huysmans M. Drought propagation and its impact on
667 groundwater hydrology of wetlands: a case study on the Doode Bemde nature reserve (Belgium), Nat. Hazards
668 Earth Syst. Sci., 21, 39-51. <https://doi.org/10.5194/nhess-21-39-2021>, 2021.

669 Wu G, Chen J, Shi X, Kim J-S, Xia J and Zhang L. Impacts of Global Climate Warming on Meteorological and
670 Hydrological Droughts and Their Propagations, Earth's Future, 10, e2021EF002542.
671 <https://doi.org/10.1029/2021EF002542>, 2022.

672 Wu J, Yao H, Chen X, Wang G, Bai X and Zhang D. A framework for assessing compound drought events from
673 a drought propagation perspective, Journal of Hydrology, 604, 127228.
674 <https://doi.org/10.1016/j.jhydrol.2021.127228>, 2022.

675 Xu L, Chen N, Yang C, Zhang C and Yu H. A parametric multivariate drought index for drought monitoring and
676 assessment under climate change, Agricultural and Forest Meteorology, 310, 108657.
677 <https://doi.org/10.1016/j.agrformet.2021.108657>, 2021.

678 Yao Y, Fu B, Liu Y, Li Y, Wang S, Zhan T, Wang Y and Gao D. Evaluation of ecosystem resilience to drought
679 based on drought intensity and recovery time, Agricultural and Forest Meteorology, 314, 108809.
680 <https://doi.org/10.1016/j.agrformet.2022.108809>, 2022.

681 Yeh H-F and Hsu H-L. Using the Markov Chain to Analyze Precipitation and Groundwater Drought
682 Characteristics and Linkage with Atmospheric Circulation, Sustainability, 11,
683 <https://doi.org/10.3390/su11061817>, 2019.

684 Zhang Q, Miao C, Gou J, Wu J, Jiao W, Song Y and Xu D. Spatiotemporal characteristics of meteorological to
685 hydrological drought propagation under natural conditions in China, Weather and Climate Extremes, 38, 100505.
686 <https://doi.org/10.1016/j.wace.2022.100505>, 2022.

687 Zhang T, Su X, Zhang G, Wu H, Wang G and Chu J. Evaluation of the impacts of human activities on
688 propagation from meteorological drought to hydrological drought in the Weihe River Basin, China, Science of
689 The Total Environment, 819, 153030. <https://doi.org/10.1016/j.scitotenv.2022.153030>, 2022.

690 Zhang T, Su X, Wu L and Chu J. Identification of dynamic drought propagation from a nonstationary perspective
691 and its application to drought warnings, Journal of Hydrology, 626, 130372.
692 <https://doi.org/10.1016/j.jhydrol.2023.130372>, 2023.

693 Zhang Y, Hao Z, Feng S, Zhang X, Xu Y and Hao F. Agricultural drought prediction in China based on drought
694 propagation and large-scale drivers, Agricultural Water Management, 255, 107028.
695 <https://doi.org/10.1016/j.agwat.2021.107028>, 2021.

696 Zhong F, Cheng Q and Wang P. Meteorological Drought, Hydrological Drought, and NDVI in the Heihe River
697 Basin, Northwest China: Evolution and Propagation, Advances in Meteorology, 2020, 2409068.
698 <https://doi.org/10.1155/2020/2409068>, 2020.

699 Zhou J, Li Q, Wang L, Lei L, Huang M, Xiang J, Feng W, Zhao Y, Xue D, Liu C, Wei W and Zhu G. Impact of
700 Climate Change and Land-Use on the Propagation from Meteorological Drought to Hydrological Drought in the
701 Eastern Qilian Mountains, Water, 11, 1602. <https://doi.org/10.3390/w11081602>, 2019.

702 Zhou Y G, Yijie, Shi Y, Zhusuo W, Chen H and Liu Z. Risk Analysis of Drought in Guangdong—Hong Kong—
703 Macao Greater Bay Area Based on Copula Function, Journal of North China University of Water Resources and
704 Electric Power (Natural Science Edition), 43, 20-28+66. <https://doi.org/10.19760/j.ncwu.zk.2022044>, 2022. (in
705 Chinese)

706 Zhou Z, Shi H, Fu Q, Ding Y, Li T and Liu S. Investigating the Propagation From Meteorological to
707 Hydrological Drought by Introducing the Nonlinear Dependence With Directed Information Transfer Index,
708 Water Resources Research, 57, e2021WR030028. <https://doi.org/10.1029/2021WR030028>, 2021.
709